Modeling, Control and Design Optimization for a Fully-actuated Hexarotor Aerial Vehicle with Tilted Propellers

Sujit Rajappa, Markus Ryll, Heinrich H. Bülthoff, Antonio Franchi

Modeling, Control and Design Optimization for a Fully-actuated Hexarotor Aerial Vehicle with Tilted Propellers

Sujit Rajappa[1], Markus Ryll[3], Heinrich H. Bülthoff[1,2] and Antonio Franchi[3,4]

***Abstract*— Mobility of a hexarotor UAV in its standard configuration is limited, since all the propeller force vectors are parallel and they achieve only 4 DoF actuation, similar, e.g., to quadrotors. As a consequence, the hexarotor pose cannot track an arbitrary trajectory over time. In this paper, we consider a different hexarotor architecture where propellers are tilted, without the need of any additional hardware. In this way, the hexarotor possess a 6 DoF actuation which allows to independently reach positions and orientations in free space and to be able to exert forces on the environment to resist any wrench for aerial manipulation tasks. After deriving the dynamical model of the proposed hexarotor, we discuss the controllability and the tilt angle optimization to reduce the control effort. An exact feedback linearization and decoupling control law is proposed based on the input-output mapping, considering the Jacobian and task acceleration, for non-linear trajectory tracking. The robustness of our approach is validated by simulation results.**

I. INTRODUCTION

Research in the field and applications related to unmanned aerial vehicles (UAVs) has been a popular research topic in recent times, see e.g., [1] and references therein. The application possibility to use the UAV for various tasks such as search and rescue operation, exploration, surveillance, cooperative swarm tasks or transportation are all increasing and has been the main research subject with growing interest in the last decade with many industrial collaborations. Lately, the mobile manipulation tasks by aerial vehicles and physical interaction with the environment for various applications has been growing ground within the UAV community. The interaction can be done by direct contact [2]–[5], by considering simple grasping/manipulation tasks [6], [7] and has moved forward to multiple collaborative interactive UAVs [8].

Among the many challenges faced by typical UAVs, such as little flight time, limited payload capacity, uncertainties in outside environment etc., an important one is the underactuation, i.e., the inability to exert forces in some directions of the body frame. Quadrotors have been used as the main platform for applications as well as research, though they are also underactuated, i.e., they cannot exert any force parallel to the plane perpendicular to their vertical direction in body frame. This is why a quadrotor needs to roll and pitch to move in any direction.

But when it comes to physical interaction, underactuation might become a serious problem for the capabilities and overall stabilization of the aerial vehicle. As the application complexity is going higher, major breakthroughs and advancements in innovative mechanical designs, actuation concepts, micro-electro mechanical systems, sensor technology and power capacity is always envisioned. Several possibilities have been proposed in the past literature spanning different concepts: ducted-fan designs [9], tilt-wing mechanisms [10], or tilt-rotor actuations [11], [12]. The concept of tilt-rotor architecture has been much explored to increase flight time [13] but not for the improvement of the underactuation problem. In [14] the underactuation was addressed by four additional rotors at the end of each frame in lateral position. But the position of the rotor increased the complexity of controllability because of the air flow between the vertical and the lateral rotors, resulting in non-linear dynamics along with the increase in payload.

Our own in-lab investigation led to the novel quadrotor design [15] with tilted propellers by 4 additional actuators included for the tilting thereby creating the possibility to regulate independently the 6 DoFs of the platform. Though underactuation problem was solved by this design, the need of tilting the propellers in order to resist to any external wrench makes it tough for the aerial manipulation task, where forces shall be exerted instantaneously to resist to unexpected external wrenches. Additionally, the use of servomotors for tilting the propellers makes the overall model challenging to control in real scenarios involving physical interaction.

In [16], a hexarotor with the propellers rotated about one axis was suggested. Our approach is different, as we present a more general tilt design, a control law for 6 DoFs trajectory tracking, a methodology to optimize the fixed tilting angles for each propeller depending on the task in exam and an improved mechanical design where all the propellers lie in the same plane.

Taking inspiration from all the related work, we propose a novel hexarotor with tilted propeller design, where each rotor is fixedly mounted in a configuration that is rotated about two possible axes. The main objective of this work is full controllability of the UAV's position and orientation by means of tilted propellers, thereby making it completely actuated. The full actuation comes with the cost of a more advanced mechanical design.

The focus and structure of this paper is therefore: (i)

[1]Max Planck Institute for Biological Cybernetics, Spemannstraße 38, 72076 Tübingen, Germany, {sujit.rajappa}{hhb}@tue.mpg.de

[2]Department of Brain and Cognitive Engineering, Korea University, Anam-dong, Seongbuk-gu, Seoul, 136-713 Korea.

[3]CNRS, LAAS, 7 avenue du colonel Roche, F-31400 Toulouse, France mryll@laas.fr, afranchi@laas.fr

[4]Univ de Toulouse, LAAS, F-31400 Toulouse, France

This work has been partially supported by the European Community under Contract ICT 287617 ARCAS.

to discuss in detail and derive the dynamic model for the proposed hexarotor in Sec. II, (ii) to devise and develop the closed-loop controller for the hexarotor which is able to asymptotically track an arbitrary desired trajectory for the position and orientation in 3 dimensional free space in Sec. III, (iii) to optimize the propeller tilt angles depending on the application/trajectory to reduce the overall control effort in the Sec. IV, (iv) to start the design of a novel and feasible hexarotor architecture with tilted propellers in Sec. V, and finally (v) to test the hexarotor model and its theoretical concepts in simulation, presented in Sec. VI. Conclusions and future perspectives are given in Sec. VII.

II. DESIGN AND MODELING

A standard hexarotor possesses six propellers that are all rotating about six parallel axes. Even though this choice increases redundancy and payload, such configuration has an underactuated dynamics similar to a standard quadrotor. In fact, the six propellers create an input force that is always parallel to that axis, no matter the values of the six rotational speeds. In this case a change of the direction of the input force can only be obtained by reorienting the whole vehicle. Therefore, the desired output trajectory can only be defined by a 4-dimensional output, namely the center of mass (CoM) 3D position plus the yaw angle, despite the presence of 6 control inputs. In fact in [17] it has been proven that such kind of systems are exactly linearizable with a dynamic feedback using as linearizing output, i.e. the CoM position and the yaw angle. Feedback linearizability also implies that the system is differentially flat and that the linearizing output is the flat output [18]. The remaining two configuration variables, i.e., the roll and pitch angles, cannot be chosen at will, since they are being determined by the desired trajectory of the CoM, the yaw angle, and their derivatives.

On the converse, the goal of the hexarotor modeling approach presented here is to exploit at best the six available inputs, thus resulting in a system that is fully actuated, i.e., linear and angular accelerations can be set independently acting on the six inputs. In order to obtain full actuation, we remove the constraint for the propellers to rotate about six parallel axes, so that a force in any direction can be generated regardless of the vehicle orientation. Thanks to full actuation, this hexarotor can follow desired 6-DoFs trajectories comprising both the CoM position and, independently, the vehicle orientation described, e.g., by roll, pitch, and yaw, or by a rotation matrix.

Even though a reallocation and reorientation of the six propellers allows for more design flexibility it also increases the number of design parameters thus increasing the design complexity. In order to find a good compromise between full actuation and low number of model parameters, we decide to add some constraints on the parameters, i.e.:

- the CoM and the six propeller centers are coplanar, like in a standard hexarotor;
- the propeller centers lie on lines that intersect with the CoM and form 6 equal angles of $\pi/3$ each;

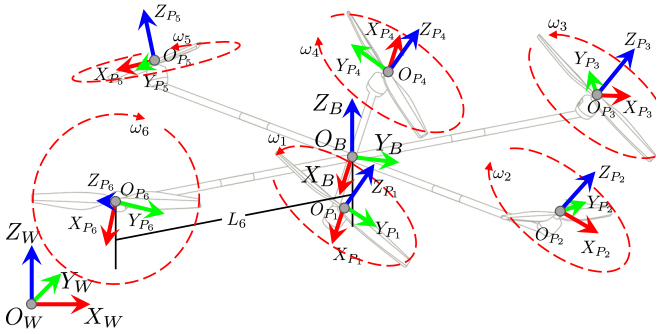

Fig. 1: Schematic representation of the hexarotor described in this paper.

- the tilted planes of the propellers are coordinated, in the sense that, each pair of propellers ((1)-(2), (3)-(4), (5)-(6)) are tilted oppositely about the X- and Y-axis. Detailed explanation can be found in Section IV;

These three design choices simplify the design complexity while still allowing a full spectrum of actuation capabilities, as it will be shown in the paper. In the following we formally describe our hexarotor model and all the related design choices.

A. Static System Description

We denote the world inertial frame with $\mathcal{F}_W : \{\boldsymbol{O}_W - \boldsymbol{X}_W\boldsymbol{Y}_W\boldsymbol{Z}_W\}$ and with $\mathcal{F}_B : \{\boldsymbol{O}_B - \boldsymbol{X}_B\boldsymbol{Y}_B\boldsymbol{Z}_B\}$ the body frame attached to the hexarotor frame, where $\boldsymbol{O}_B$ coincides with the hexarotor CoM. Let the frame associated with the i-th propeller be defined as $\mathcal{F}_{P_i} : \{\boldsymbol{O}_{P_i} - \boldsymbol{X}_{P_i}\boldsymbol{Y}_{P_i}\boldsymbol{Z}_{P_i}\}$, where $i = 1 \dots 6$. The origin $\boldsymbol{O}_{P_i}$ coincides with the center of spinning and the CoM of the i-th propeller, the axes $\boldsymbol{X}_{P_i}$ and $\boldsymbol{Y}_{P_i}$ define the rotation plane of the propeller, and $\boldsymbol{Z}_{P_i}$ is the axis about which the propeller spins and coincides with the generated thrust force. The propeller frame $\mathcal{F}_{P_i}$ is rigidly attached to the hexarotor frame, rather than to the propeller, which spins about $\boldsymbol{Z}_{P_i}$. In fact, only the direction of the force and torque exerted by the propeller are relevant to our problem. The actual spinning angle of each propeller is not important for the motion, as it will be explained in Sec. II-B.

We shall denote simply by $\boldsymbol{p} \in \mathbb{R}^3$ the position of $\boldsymbol{O}_B$ in $\mathcal{F}_W$, and by ${}^B\boldsymbol{p}_i \in \mathbb{R}^3$ the position of $\boldsymbol{O}_{P_i}$ in $\mathcal{F}_B$, with $i = 1 \dots 6$. We make the following design choice:

$$ {}^B\boldsymbol{p}_i = \boldsymbol{R}_Z\left((i-1)\frac{\pi}{3}\right)\begin{bmatrix} L_{x_i} \\ 0 \\ 0 \end{bmatrix}, \quad \forall i = 1 \dots 6 \qquad (1) $$

where $\boldsymbol{R}_Z(\cdot)$ is the canonical rotation matrix about a Z-axis and $L_{x_i} > 0$ is the distance between $\boldsymbol{O}_{P_i}$ and $\boldsymbol{O}_B$. It is important to note that the parameter L_{x_i} is chosen depending on the strength of propeller, size of hexarotor, payload needs and doesn't affect the full-actuation of hexarotor. Furthermore, we chose $L_{x_1} = L_{x_4}$, $L_{x_2} = L_{x_5}$ and $L_{x_3} = L_{x_6}$. With these choices of $\boldsymbol{R}_Z(\cdot)$ and L_{x_i}, the $\boldsymbol{O}_{P_i}$ of the 6 propellers lie on the $\boldsymbol{X}_B\boldsymbol{Y}_B$ plane and are evenly angularly distributed, having a symmetric configuration in normal hovering position.

Symbols	Definitions
m	total mass of the hexarotor
g	gravity constant
$\boldsymbol{O}_B$	Center of hexarotor or Center of Mass (CoM)
$\boldsymbol{O}_{P_i}$	Center of the each propeller group
$\boldsymbol{p}$	position of $\boldsymbol{O}_B$ (the CoM) in $\mathcal{F}_W$
L_{x_i}	distance between $\boldsymbol{O}_{P_i}$ and $\boldsymbol{O}_B$
$\mathcal{F}_W$	inertial world frame
$\mathcal{F}_B$	hexarotor body frame
$\mathcal{F}_{P_i}$	i-th propeller frame
${}^W\boldsymbol{R}_B$	rotation matrix from $\mathcal{F}_B$ to $\mathcal{F}_W$
${}^B\boldsymbol{R}_{P_i}$	rotation matrix from $\mathcal{F}_{P_i}$ to $\mathcal{F}_B$
$\boldsymbol{I}_B$	inertia of the hexarotor frame
k_f	propeller thrust coefficient
k_m	propeller drag coefficient
α_i	i-th propeller tilt angle about $\overline{\boldsymbol{O}_{P_i}\boldsymbol{O}_B}$
β_i	i-th propeller tilt angle about $\boldsymbol{Y}_{P_i}$
$\bar{\omega}_i$	i-th propeller spinning velocity about $\boldsymbol{Z}_{P_i}$
$\boldsymbol{\omega}_B$	angular velocity of $\mathcal{F}_B$ w.r.t. $\mathcal{F}_W$ expressed in $\mathcal{F}_B$
$\boldsymbol{\tau}_{\text{ext}}$	external disturbance torque acting on the hexarotor
$\boldsymbol{T}_{\text{thrust}_i}$	i-th propeller thrust along $\boldsymbol{Z}_{P_i}$
$\boldsymbol{T}_{\text{drag}_i}$	drag due to the i-th propeller along $\boldsymbol{Z}_{P_i}$

TABLE I: Main symbols used in the paper

Let the rotation matrix ${}^W\boldsymbol{R}_B \in SO(3)$ represent the orientation of $\mathcal{F}_B$ w.r.t. $\mathcal{F}_W$ and ${}^B\boldsymbol{R}_{P_i} \in SO(3)$ represent the orientation of $\mathcal{F}_{P_i}$ w.r.t. $\mathcal{F}_B$, for $i = 1 \dots 6$. In order to obtain a minimal parameterization of the propeller orientation we decompose each ${}^B\boldsymbol{R}_{P_i}$ in three consecutive rotations

$$ {}^B\boldsymbol{R}_{P_i} = \boldsymbol{R}_Z\left(\tfrac{(i-1)\pi}{3}\right)\boldsymbol{R}_X(\alpha_i)\boldsymbol{R}_Y(\beta_i), \quad \forall i = 1 \dots 6 \quad (2) $$

where the angular parameters α_i and β_i represent the tilt angles, that uniquely define the rotation plane of the i-th propeller, $\boldsymbol{X}_{P_i}\boldsymbol{Y}_{P_i}$ or, equivalently, the direction of $\boldsymbol{Z}_{P_i}$ in $\mathcal{F}_B$. The angles α_i and β_i have a clear geometrical interpretation, in fact the i-th propeller plane $\boldsymbol{X}_{P_i}\boldsymbol{Y}_{P_i}$ is obtained from $\boldsymbol{X}_B\boldsymbol{Y}_B$ by first applying a rotation of α_i about the line $\overline{\boldsymbol{O}_B\boldsymbol{O}_{P_i}}$ and then a rotation of β_i about $\boldsymbol{Y}_{P_i}$, which lies on $\boldsymbol{X}_B\boldsymbol{Y}_B$ and is perpendicular to $\overline{\boldsymbol{O}_B\boldsymbol{O}_{P_i}}$. The α_i and β_i rotation is pictorially represented in Fig. 2.

For convenience, we group the tilting angles in two 6-tuples: $\boldsymbol{\alpha} = (\alpha_1, \alpha_2, \alpha_3, \alpha_4, \alpha_5, \alpha_6)$ and $\boldsymbol{\beta} = (\beta_1, \beta_2, \beta_3, \beta_4, \beta_5, \beta_6)$. Considering the design constrains explained earlier in Section II, the tilt w.r.t. $\boldsymbol{X}_{P_i}$ is fixed as $\alpha_1 = -\alpha_2 = \alpha_3 = -\alpha_4 = \alpha_5 = -\alpha_6$ and w.r.t $\boldsymbol{Y}_{P_i}$ is $\beta_1 = -\beta_2 = \beta_3 = -\beta_4 = \beta_5 = -\beta_6$ in a co-ordinated way. The angle of tilt is further detailed in optimization (Section IV).

In this paper we consider the case in which $L_{x_i}, \alpha_i, \beta_i$, for $i = 1 \dots 6$, are constant during flight, but can be changed during a pre-flight setup, in order, e.g., to minimize the sum of the overall control effort for a specific task, as shown in Sec. IV.

B. Equations of Motion

Utilizing the standard Newton-Euler approach for dynamic systems, it is possible to derive the complete dynamic equations of the hexarotor by considering the forces and torques that are generated by each propeller rotation together with the significant gyroscopic and inertial effects. In the following we recap the standard[1] assumptions that we are considering here:

- $\boldsymbol{O}_B$ coincides with the CoM of the hexarotor;
- $\boldsymbol{O}_{P_i}$ coincides with the CoM of the i-th propeller;
- the motors actuating the six propellers implement a fast high-gain local controller which is able to impose a desired spinning speed with negligible transient, thus allowing to consider the spinning rates as (virtual) control inputs in place of the motor torques;
- gyroscopic and inertial effects due to the propellers and the motors are considered as second-order disturbances to be rejected by the feedback nature of the controller;
- the tilted propellers might cause additional turbulences due to the possible intersection of the airflows. These turbulences are considered as negligible as the possible intersection of the airflows happens not close to the propellers. In fact, tilt configurations have been already proven to be feasible in reality [19].

We will test in simulation (see Section VI) the practicability of these assumptions with the proposed controller on a dynamic model which includes the aforementioned unmodeled effects.

For ease of presentation, in the following we shall express the translational dynamics in $\mathcal{F}_W$ where as the rotational dynamics is expressed in $\mathcal{F}_B$.

1) Rotational dynamics: Denote with $\boldsymbol{\omega}_B \in \mathbb{R}^3$ the angular velocity of $\mathcal{F}_B$, with respect to $\mathcal{F}_W$, expressed in $\mathcal{F}_B$. Then the rotational dynamics is

$$ \boldsymbol{I}_B\dot{\boldsymbol{\omega}}_B = -\boldsymbol{\omega}_B \times \boldsymbol{I}_B\boldsymbol{\omega}_B + \boldsymbol{\tau} + \boldsymbol{\tau}_{\text{ext}}, \quad (3) $$

where $\boldsymbol{I}_B$ is the hexarotor body inertia matrix, $\boldsymbol{\tau}_{\text{ext}}$ accounts for external disturbances and unmodeled effects, and $\boldsymbol{\tau}$ is the input torque, which is decomposed in

$$ \boldsymbol{\tau} = \boldsymbol{\tau}_{\text{thrust}} + \boldsymbol{\tau}_{\text{drag}}, \quad (4) $$

where $\boldsymbol{\tau}_{\text{thrust}}$ is produced by the six propeller thrusts and $\boldsymbol{\tau}_{\text{drag}}$ is due to the six propeller drags. The two individual components of (4) are discussed in detail below.

a) Torque due to thrusts ($\boldsymbol{\tau}_{\text{thrust}}$): The i-th propeller creates a force vector applied at $\boldsymbol{O}_{P_i}$ and directed along $\boldsymbol{Z}_{P_i}$, which is expressed in $\mathcal{F}_{P_i}$ by

$$ \boldsymbol{T}_{\text{thrust}_i} = \begin{bmatrix} 0 & 0 & k_f\bar{\omega}_i^2 \end{bmatrix}^T \quad (5) $$

where $k_f > 0$ is a constant thrust coefficient and $\bar{\omega}_i$ is the spinning velocity of the i-th propeller. The thrust torque, expressed in $\mathcal{F}_B$ is then

$$ \boldsymbol{\tau}_{\text{thrust}} = \sum_{i=1}^{6} \left({}^B\boldsymbol{p}_i \times {}^B\boldsymbol{R}_{P_i}\boldsymbol{T}_{\text{thrust}_i} \right). \quad (6) $$

b) Torque due to drag ($\boldsymbol{\tau}_{\text{drag}}$): The drag moment generated by the i-th propeller acts in the opposite direction of the propeller angular velocity and is expressed in $\mathcal{F}_{P_i}$ by

$$ \boldsymbol{T}_{\text{drag}_i} = \begin{bmatrix} 0 & 0 & (-1)^i k_m\bar{\omega}_i^2 \end{bmatrix}^T, \quad (7) $$

[1]Similar assumptions have been used, e.g., in [13]–[15]

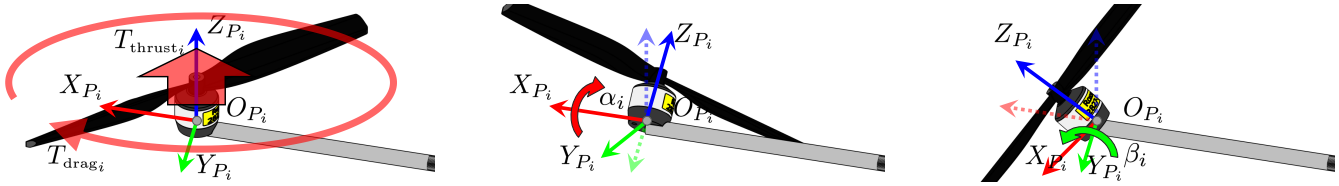

Fig. 2: (a): i-th hexarotor arm presenting body frame $\mathcal{F}_{P_i}$ and the generated thrust T_{thrust_i} and drag T_{drag_i}; (b) and (c): Visualization of the possible reorientation of the propeller around X_{P_i} (case (b)) and Y_{P_i} (case (c)). The angle of reorientation is denoted with α in (b) and β in (c)

where $k_m > 0$ is the propeller drag coefficient. The factor $(-1)^i$ is used since half of the propellers rotate clockwise and the other half rotates counter-clockwise. This is done in order to have an automatic counterbalance of the drag torques at hovering. The drag torque due to the six propellers expressed in $\mathcal{F}_B$ is then

$$\boldsymbol{\tau}_{\text{drag}} = \sum_{i=1}^{6} {}^{B}\boldsymbol{R}_{P_i}\, \boldsymbol{T}_{\text{drag}_i}. \tag{8}$$

Putting together (8) and (6) in (4) we can write

$$\boldsymbol{\tau} = \boldsymbol{\tau}(\boldsymbol{\alpha}, \boldsymbol{\beta})\boldsymbol{u}, \tag{9}$$

where $\boldsymbol{\tau}(\boldsymbol{\alpha}, \boldsymbol{\beta}) \in \mathbb{R}^{3\times 6}$ is the Jacobian matrix that relates the input torque $\boldsymbol{\tau}$ to the control input

$$\boldsymbol{u} = [\bar{\omega}_1^2 \;\; \bar{\omega}_2^2 \;\; \bar{\omega}_3^2 \;\; \bar{\omega}_4^2 \;\; \bar{\omega}_5^2 \;\; \bar{\omega}_6^2]^T \in \mathbb{R}^{6\times 1}, \tag{10}$$

i.e., the squares of the rotational speeds of each propeller.

2) Translational dynamics: Thanks to the assumption on the location of the hexarotor and propeller centers of mass, we can express the translational dynamics in $\mathcal{F}_W$, using the standard Newton-Euler formulation, as

$$m\ddot{\boldsymbol{p}} = m \begin{bmatrix} 0 \\ 0 \\ -g \end{bmatrix} + {}^{W}\boldsymbol{R}_B \boldsymbol{F}(\boldsymbol{\alpha}, \boldsymbol{\beta})\boldsymbol{u} + \boldsymbol{f}_{\text{ext}} \tag{11}$$

where $\boldsymbol{f}_{\text{ext}}$ represents external disturbances and unmodeled effects, and $\boldsymbol{F}(\boldsymbol{\alpha}, \boldsymbol{\beta}) \in \mathbb{R}^{3\times 6}$ is the Jacobian matrix that relates $\boldsymbol{u}$ with the total force produced by the propellers (expressed in body frame), i.e.,

$$F(\boldsymbol{\alpha}, \boldsymbol{\beta})\boldsymbol{u} = \sum_{i=1}^{6} {}^{B}\boldsymbol{R}_{P_i}\, \boldsymbol{T}_{\text{thrust}_i}. \tag{12}$$

Notice that in a standard hexarotor $\alpha_i = \beta_i = 0$, for all $i = 1 \dots 6$. This implies that $F(\boldsymbol{\alpha}, \boldsymbol{\beta})$ has rank equal to one (the total force is always directed on the $\boldsymbol{Z}_B$ axis).

III. CONTROL DESIGN

The control problem considered here is an output tracking problem. In particular, the hexarotor is tasked to track, simultaneously, a desired trajectory $\boldsymbol{p}_d(t)$ with the CoM position $\boldsymbol{p}$ and a given orientation $\boldsymbol{R}_d(t)$ with the body orientation ${}^{W}\boldsymbol{R}_B$. The available control inputs are the six spinning rates of the propellers $\boldsymbol{u}$ defined in (10).

Neglecting the external forces and torques (which are handled by the feedback nature of the control) we rewrite here the hexarotor dynamical model, that is used for the control design

$$\ddot{\boldsymbol{p}} = \begin{bmatrix} 0 & 0 & -g \end{bmatrix}^T + \frac{1}{m} {}^{W}\boldsymbol{R}_B \boldsymbol{F}(\boldsymbol{\alpha}, \boldsymbol{\beta})\boldsymbol{u} \tag{13}$$

$$\dot{\boldsymbol{\omega}}_B = -\boldsymbol{I}_B^{-1}(\boldsymbol{\omega}_B \times \boldsymbol{I}_B\boldsymbol{\omega}_B) + \boldsymbol{I}_B^{-1}\boldsymbol{\tau}(\boldsymbol{\alpha}, \boldsymbol{\beta})\boldsymbol{u} \tag{14}$$

$${}^{W}\dot{\boldsymbol{R}}_B = {}^{W}\boldsymbol{R}_B[\boldsymbol{\omega}_B]_\wedge \tag{15}$$

with $[\cdot]_\wedge$ being the usual map from $\mathbb{R}^3$ to $so(3)$.

A. Exact Feedback Linearization and Decoupling Control

In order to apply a feedback linearization technique we rewrite (13)–(14) in a matricial form

$$\begin{bmatrix} \ddot{\boldsymbol{p}} \\ \dot{\boldsymbol{\omega}}_B \end{bmatrix} = \boldsymbol{f} + \boldsymbol{J}_R \left[\bar{\boldsymbol{J}}(\boldsymbol{\alpha}, \boldsymbol{\beta})\right] \boldsymbol{u} = \boldsymbol{f} + \boldsymbol{J}(\boldsymbol{\alpha}, \boldsymbol{\beta})\boldsymbol{u} \tag{16}$$

where $\boldsymbol{f} \in \mathbb{R}^6$ is the drift vector due to the gravity and the rotational inertia, $\boldsymbol{J}_R = \begin{bmatrix} \frac{1}{m}{}^{W}\boldsymbol{R}_B & \boldsymbol{0} \\ \boldsymbol{0} & \boldsymbol{I}_B^{-1} \end{bmatrix} \in \mathbb{R}^{6\times 6}$, $\bar{\boldsymbol{J}}(\boldsymbol{\alpha}, \boldsymbol{\beta}) = \begin{bmatrix} \boldsymbol{F}(\boldsymbol{\alpha}, \boldsymbol{\beta}) \\ \boldsymbol{\tau}(\boldsymbol{\alpha}, \boldsymbol{\beta}) \end{bmatrix} \in \mathbb{R}^{6\times 6}$, and the 6×6 matrix $\boldsymbol{J}(\boldsymbol{\alpha}, \boldsymbol{\beta})$ will be referred to as the input Jacobian[2].

If $\boldsymbol{J}(\boldsymbol{\alpha}, \boldsymbol{\beta})$ is invertible we choose the control input as

$$\boldsymbol{u} = \boldsymbol{J}^{-1}(\boldsymbol{\alpha}, \boldsymbol{\beta})\left(-\boldsymbol{f} + \boldsymbol{v}\right) \tag{17}$$

where $\boldsymbol{v}$ is an additional input, thus obtaining

$$\begin{bmatrix} \ddot{\boldsymbol{p}} \\ \dot{\boldsymbol{\omega}}_B \end{bmatrix} = \boldsymbol{v} = \begin{bmatrix} \boldsymbol{v}_p \\ \boldsymbol{v}_R \end{bmatrix}, \tag{18}$$

i.e. the system is exactly linearized via a static feedback. Fig. 3 shows the control scheme architecture.

In order to obtain an exponential convergence to $\boldsymbol{0}$ of the position error $\boldsymbol{p} - \boldsymbol{p}_d = \boldsymbol{e}_{\boldsymbol{p}}$ one can choose a linear controller

$$\boldsymbol{v}_p = \ddot{\boldsymbol{p}}_d - \boldsymbol{K}_{p1}\dot{\boldsymbol{e}}_{\boldsymbol{p}} - \boldsymbol{K}_{p2}\boldsymbol{e}_{\boldsymbol{p}} - \boldsymbol{K}_{p3}\int_{t_0}^{t} \boldsymbol{e}_{\boldsymbol{p}}, \tag{19}$$

where the diagonal positive definite gain matrixes $\boldsymbol{K}_{p_1}$, $\boldsymbol{K}_{p_2}$, $\boldsymbol{K}_{p_3}$ define Hurwitz polynomials.

Now considering the orientation tracking, a popular used parameterization is to resort to Euler angles. However it is well known that they are prone to singularity problems. Keeping this in mind, the controller for the rotational configuration is developed directly on $so(3)$ and thereby it avoids

[2]In standard hexarotor the input Jacobian $\boldsymbol{J}(\boldsymbol{\alpha}, \boldsymbol{\beta})$ has rank equal to four similar to a quadrotor.

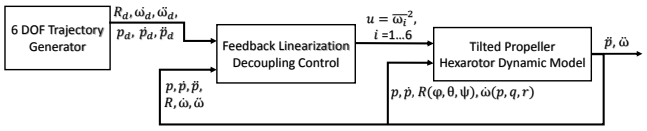

Fig. 3: Control scheme architecture

any singularities that arise in local coordinates, such as Euler angles. Now assuming that $\boldsymbol{R}_d(t) \in \mathcal{C}^3$ and $\boldsymbol{\omega}_d = [\boldsymbol{R}_d^T \dot{\boldsymbol{R}}_d]_\vee$, where $[\cdot]_\vee$ represents the inverse map from $so(3)$ to $\mathbb{R}^3$, the attitude tracking error $\boldsymbol{e}_R \in \mathbb{R}^3$ is defined similarly to [20] as

$$\boldsymbol{e_R} = \frac{1}{2}[\boldsymbol{R}_d^{TW}\boldsymbol{R}_B - {}^W\boldsymbol{R}_B^T\boldsymbol{R}_d]_\vee, \tag{20}$$

and the tracking error of the angular velocity $\boldsymbol{e}_\omega \in \mathbb{R}^3$ is given by

$$\boldsymbol{e_\omega} = \boldsymbol{\omega}_B - {}^W\boldsymbol{R}_B^T\boldsymbol{R}_d\boldsymbol{\omega}_d. \tag{21}$$

In order to obtain an asymptotic convergence to $\mathbf{0}$ of the rotational error $\boldsymbol{e}_R$ one can choose the following controller

$$\boldsymbol{v}_R = \dot{\boldsymbol{\omega}}_d - \boldsymbol{K}_{R_1}\boldsymbol{e}_\omega - \boldsymbol{K}_{R_2}\boldsymbol{e}_R - \boldsymbol{K}_{R_3}\int_{t_0}^{t}\boldsymbol{e}_R \tag{22}$$

where the diagonal positive definite gain matrixes $\boldsymbol{K}_{R_1}$, $\boldsymbol{K}_{R_2}$, $\boldsymbol{K}_{R_3}$ define Hurwitz polynomials also in this case.

B. Discussion on the Invertibility of $\boldsymbol{J}(\boldsymbol{\alpha}, \boldsymbol{\beta})$

The previous control design relies on the invertibility of the matrix $\boldsymbol{J}(\boldsymbol{\alpha}, \boldsymbol{\beta})$. To have the 6 DoFs, it is necessary to create acceleration in all direction (i.e. $\ddot{x}, \ddot{y}, \ddot{z}, \dot{p}, \dot{q}, \dot{r}$). This is possible only if the Jacobian matrix $\boldsymbol{J}(\boldsymbol{\alpha}, \boldsymbol{\beta})$ in (17) is invertible at all time instances. This implies $\rho_J = rank(\boldsymbol{J}(\boldsymbol{\alpha}, \boldsymbol{\beta})) = rank(\boldsymbol{J}_R.\bar{\boldsymbol{J}}(\boldsymbol{\alpha}, \boldsymbol{\beta})) \equiv rank(\bar{\boldsymbol{J}}(\boldsymbol{\alpha}, \boldsymbol{\beta})) = 6,\ \forall t > 0$. Here $\boldsymbol{J}_R$ is a nonsingular square matrix as seen in (16) and therefore doesn't affect $rank(\boldsymbol{J}(\boldsymbol{\alpha}, \boldsymbol{\beta}))$. Therefore $\bar{\boldsymbol{J}}(\boldsymbol{\alpha}, \boldsymbol{\beta})$ is the only rank affecting component and is directly dependent on the propeller tilting configuration $\boldsymbol{\alpha}_i$ and $\boldsymbol{\beta}_i$. Necessary conditions for α_i and β_i are:

- $\alpha_i \neq \pm\pi/2$, where $rank(\bar{\boldsymbol{J}}(\boldsymbol{\alpha}, \boldsymbol{\beta})) < 6\ \forall\ \beta_i$.

Due to the high non linearity of $\bar{\boldsymbol{J}}(\boldsymbol{\alpha}, \boldsymbol{\beta})$ sufficient conditions for the invertibility are hard to find. Figure 4 shows $\det(\bar{\boldsymbol{J}}(\boldsymbol{\alpha}, \boldsymbol{\beta}))$ of the presented prototype in Sec.V. All combinations lying in the XY-plane are no feasible solutions.

IV. OPTIMIZATION

The angles α_i and β_i for $i = 1 \ldots 6$ are adjusted during the pre-flight setup as described in Sec. II. This gives the possibility to change the angles depending on the needs of a particular trajectory. In this section, we consider this capability to optimize the angles α_i and β_i depending on a predefined desired trajectory to reduce the control effort. As a reminder, the main motive is the full controllability in position and orientation. This comes with the cost of a higher control effort. The objective of this section is therefore to reduce this parasitic effect.

The predominant energy consuming parts of the hexarotor are the propeller motors. Minimizing the control effort

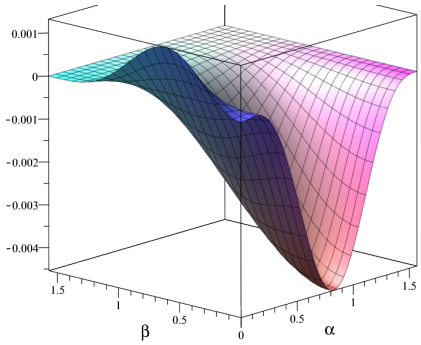

Fig. 4: Determinant value (z-axis) of $\bar{\boldsymbol{J}}(\boldsymbol{\alpha}, \boldsymbol{\beta})$ of the presented prototype

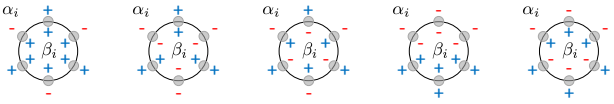

1.3e7	1.0e6	1.1e6	no feasible solution	no feasible solution
(a)	(b)	(c)	(d)	(e)

TABLE II: Stylized tested configuration and results. First row: Different configuration presented. Outside the circle the sign of α_i is indicated, within the circle the sign of β_i is indicated. Second row: Value of the optimized $\int ||\omega||_{min}$. Configuration (b) is the best configuration for the given trajectory. Configurations (d) and (e) are not feasible configurations

through the norm of the control output $||\boldsymbol{u}||$ by optimizing the particular α_i and β_i will as well reduce the energy consumption in flight. To reduce the complexity of the optimization, α_i and β_i shall be changed in a coordinated way as explained before. We decided to use the same α' and β' respectively for α_i and $\beta_i \in i = 1 \ldots 6$, but with different signs for the individual joints. An overview of the compared configurations can be found in table II. The coordinated variation of α_i and β_i offers two additional advantages: (i) no asymmetries in the hexarotor body and (ii) no or a minimum change of the CoM. Considering these constraints, the optimization problem can be defined as:

$$\min_{\alpha,\beta}\int_0^{t_f}||\boldsymbol{u}||\mathrm{d}t \tag{23}$$

Subject to:

$$0 < \alpha' < \frac{\pi}{2} \tag{24}$$

$$0 < \beta' < \frac{\pi}{2} \tag{25}$$

$$0 < \bar{\omega}_i \text{ , for } i \in 1..6 \tag{26}$$

Here (24) and (25) are defining the lower and upper bounds for α_i and β_i, while (26) ensures a positive rotation speed $\bar{\omega}_i$ for all propellers. The presented minimization problem is a multi-dimensional constrained nonlinear optimization problem and can be solved using the in-build optimization capabilities of MATLAB by exploiting the *fmincon*-function [21].

To compare (minimal control effort) the different configurations shown in table II, we used the presented optimization

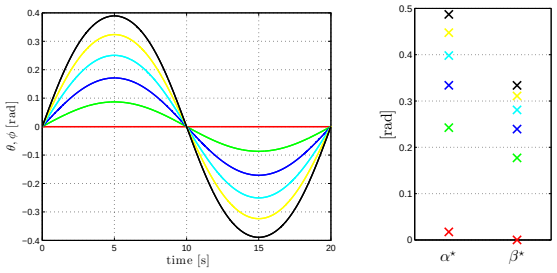

(a) (b)

Fig. 5: (a): Desired sinusoidal trajectories for equal θ and ϕ. Their amplitude is increased in six steps from 0° (0 rad) to 22.5° ($\approx$ 0.39 rad); all other values remain constant ($=0$). (b): Optimal values for α and β corresponding to the six trajectories presented in (a)

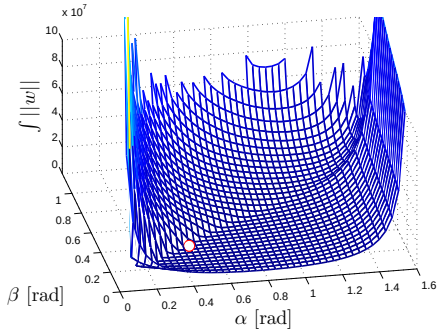

Fig. 6: Objective function for a given trajectory. Optimum is marked with a red circle

technique to find the optimal values $\alpha^\star$ and $\beta^\star$ and the associated $\int ||\omega||_{min}$. As trajectory, a typical flight regime has been chosen, which is presented in Section VI-A. The minimum value of the objective function could be found in configuration (b). Therefore all further experiments will be performed by using this configuration: $\alpha' = \alpha_1 = -\alpha_2 = \alpha_3 = -\alpha_4 = \alpha_5 = -\alpha_6$ and $\beta' = \beta_1 = -\beta_2 = \beta_3 = -\beta_4 = \beta_5 = -\beta_6$.

The optimal angles α' and β' are highly dependent on the desired trajectory. To visualize the influence we conducted a trajectory, where the hexarotor hovers in place but performs a sinusoidal rotation around θ and ϕ at the same time (see figure 5 (a)). The magnitude of the rotation is increased in 6 steps up to 22.5°. α' and β' are increasing accordingly from almost zero values to $\alpha' = 0.49$ rad and $\beta' = 0.33$ rad for the maximum amplitude.

Figure 6 shows the influence of the optimization itself. For the considered sinusoidal trajectory, we calculated the value of the objective function for a wide variety of α' and β'. The optimal value is marked by a red circle in Fig. 6.

V. TILTED PROPELLER HEXAROTOR DESIGN

In order to independently control the six DoFs of the UAV, e.g., for tracking a desired position $\boldsymbol{p}_d(t)$ and orientation $\boldsymbol{R}_d(t)$, the UAV needs to have at least six actuators.

Here we have designed a novel hexarotor architecture with the design concepts discussed in Section II. The six propellers are tilted α_i w.r.t. $\boldsymbol{X}_{P_i}$ and β_i w.r.t. $\boldsymbol{Y}_{P_i}$ as seen

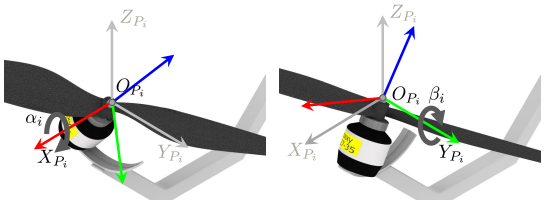

(a) (b)

Fig. 7: (a) and (b): Visualization of the possible reorientation of the propeller around X_{P_i} (case (a)) and Y_{P_i} (case (b)). The angle of reorientation is denoted with α_i in (a) and β_i in (b)

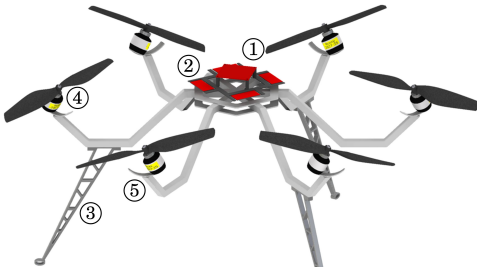

Fig. 8: CAD model of the hexarotor with tilted propellers. It is composed of: (1) Micro controller, (2) Brushless controller, (3) Lander, (4) Propeller motor, (5) Tilting set-up.

in the Fig. 7. Generally the complexity of such a tilt model would alter the point where the force and torque acts (i.e., the origin of each propeller $\boldsymbol{O}_{P_i}$), into a different plane for each propeller $\boldsymbol{P}_i$, thereby making the hexarotor model asymmetric and indirectly increasing the complexity of the system dynamics. A similar problem existed in [16]. As shown in Fig. 8, here we have designed the tilting mechanism such that the thrust forces generated by each propeller are in the same point with respect to the main body after tilting. It must be noted here that $\boldsymbol{O}_{P_i}$(point in which thrust force acts) of each propeller frame $\mathcal{F}_{P_i}$ are in the same plane $\boldsymbol{X}_B\boldsymbol{Y}_B$ as the origin $\boldsymbol{O}_B$ of hexarotor body.

Each propeller is mounted in an arc frame which is free to rotate in $\boldsymbol{X}_{P_i}$ and $\boldsymbol{Y}_{P_i}$, so that the tilt angle of α_i and β_i can be fixed as desired. The radius of the arc(R_{arc}) is designed equal to the length of the motor (with the propeller attached), so that $\boldsymbol{O}_{P_i}$ always stays at the same location in the $\boldsymbol{X}_B\boldsymbol{Y}_B$ plane with only its direction vector $[\boldsymbol{X}_{P_i}\ \ \boldsymbol{Y}_{P_i}\ \ \boldsymbol{Z}_{P_i}]^T$ changing according to the α_i and β_i orientation. The origin $\boldsymbol{O}_{P_i}$ of each propeller frame is equally spaced with 60° between each other from the center of the body frame $\boldsymbol{O}_B$ to have a symmetric configuration in normal hovering position. It must be noted that the alternating propellers are rotating in clockwise and counter-clockwise rotations, through which the torque produced by each motor shares the same direction with the motor force's in-plane components. The arm in which each propeller set-up is suspended is designed to have a curved architecture with the radius of the curvature, more than the propeller radius (R_{prop}), so that independent from the tilt of α_i and β_i, the propellers never come in contact with the arm during flight. The individual α_i and β_i are fixed following the design constrains discussed in detail in Section II. It is important to note that this hexarotor is made to freely position/orient in free space for 6 DoFs and be

able to exert force in the environment to resist any wrench for aerial manipulation task, without any additional hardware (extra payload).

VI. SIMULATIONS AND RESULTS

Here, we intend to present two simulations performed on the novel tilted propeller hexarotor, designed in Sec. II by applying the controller presented in Sec. III. We aim to prove the important contribution of the papers: (i) Hovering and reorienting the hexarotor, while maintaining a fixed position under the influence of an external force / torque disturbance, (ii) And importantly, we intend to prove the 6 DoFs this hexarotor model achieves with the proposed controller showing the robustness in a more complex trajectory tracking problem. Given the chosen $\boldsymbol{\alpha}$ and $\boldsymbol{\beta}$, not all trajectories might be feasible since the negative control outputs u_i might occur. This needs to be considered during the pre-trajectory planning step.

A. Hovering with external disturbance ($\boldsymbol{f}_{\text{ext}}/\boldsymbol{\tau}_{ext}$)

In the first simulation, we tested a hovering trajectory in which the hexarotor maintains a fixed position $\boldsymbol{p}$ but reorients itself changing at the same time the roll ϕ, pitch θ and yaw ψ angles. This involves hexarotor orienting $-12°$ w.r.t. $\boldsymbol{X}_B$, $12°$ w.r.t. $\boldsymbol{Y}_B$ axis and $15°$ w.r.t. $\boldsymbol{Z}_B$ while still hovering in the position $\boldsymbol{p} = [0 \quad 0 \quad 0]^T$. Clearly orienting w.r.t. the 3 principal body axes $\{\boldsymbol{X}_B,\ \boldsymbol{Y}_B,\ \boldsymbol{Z}_B\}$ while holding the same position is not feasible in a standard hexarotor UAV. The initial conditions were set to $\boldsymbol{p}(t_0) = \boldsymbol{0}$, $\dot{\boldsymbol{p}}(t_0) = \boldsymbol{0}$, ${}^W\boldsymbol{R}_B(t_0) = \mathbf{I}_3$ and $\boldsymbol{\omega}_B(t_0) = \boldsymbol{0}$. The desired trajectory was chosen as $\boldsymbol{p}_d(t) = 0$ and $\boldsymbol{R}_d(t) = \boldsymbol{R}_X(\phi(t))\boldsymbol{R}_Y(\theta(t))\boldsymbol{R}_Z(\psi(t))$ with $\phi(t)$, $\theta(t)$, $\psi(t)$ following the smooth profile having the maximum velocity $\dot{\theta}_{max} = 5°/\text{s}$ and the maximum acceleration $\ddot{\theta}_{max} = 2.5°/\text{s}^2$. The optimized value of $\alpha' = 13.6°$ and $\beta' = 10.6°$ obtained from Sec. IV has been used. The gains in Equations (19) and (22) were set to $\boldsymbol{K}_{p_1} = \boldsymbol{K}_{R_1} = 10\,\mathbf{I}_3$, $\boldsymbol{K}_{p_2} = \boldsymbol{K}_{R_2} = 29\,\mathbf{I}_3$ and $\boldsymbol{K}_{p_3} = \boldsymbol{K}_{R_3} = 30\,\mathbf{I}_3$.

Figures 9(a–d) show the result of hovering with external force/torque disturbance. As clearly seen in Fig. 9(c) a constant external force disturbance ($\boldsymbol{f}_{\text{ext}} = [4 \quad 2 \quad 1]^T\text{N}$) is applied, along the 3 principal axis $\{\boldsymbol{X}_B,\ \boldsymbol{Y}_B,\ \boldsymbol{Z}_B\}$, from $t = 4$ to 9s. Fig. 9(a) shows the position (current (solid line) and desired (dashed line)) brought under control while $\boldsymbol{f}_{\text{ext}}$ is applied thanks to the integral term in (19). Similarly in Fig. 9(d) a constant external torque disturbance ($\boldsymbol{\tau}_{\text{ext}} = [0.2 \quad 0.175 \quad 0.15]^T\text{Nm}$) is applied, about the 3 principal axes $\{\boldsymbol{X}_B,\ \boldsymbol{Y}_B,\ \boldsymbol{Z}_B\}$, from $t = 12$ to 18s. Fig. 9(b) shows the orientation that gets disturbed by this external torque and brought under control after a short transient, thanks to the integral term in (22). The in-zoomed Fig. 9(a) shows that the position tracking error is very minimal in powers of 10^{-9}. This simulation provides a first confirmation of the validity of the robustness of the controller during hovering with external disturbance and also the reorientation of the hexarotor while maintaining a fixed position, because of the possibility to create 6 DoFs. This point will also be addressed more thoroughly by the next simulation.

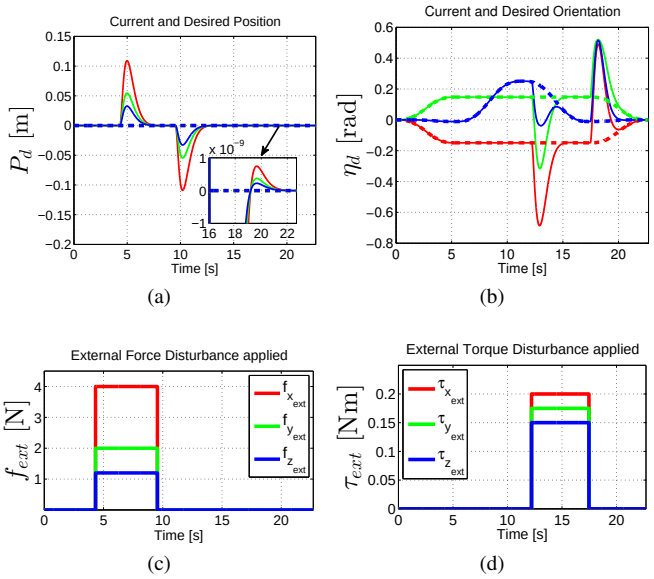

Fig. 9: Results of the hovering with external force/torque disturbance. 9(a): Desired (dashed line) and current (solid line) position $\boldsymbol{p}_d$ in x(red), y(green) and z(blue). 9(b): Desired (dashed line) and current (solid line) orientation $\boldsymbol{\eta}_d$ in roll(red), pitch(green) and yaw(blue). 9(c–d): external force($\boldsymbol{f}_{\text{ext}}$) and torque($\boldsymbol{\tau}_{\text{ext}}$) applied to the hexarotor

B. 6 DoFs trajectory tracking

In this simulation, we have addressed a more complex trajectory following a square path with vertexes $\{V_1, V_2, V_3, V_4, V_5, V_6, V_7\}$. Each vertex was associated with the following desired positions and orientations[3]

- $\boldsymbol{V}_1$: $\boldsymbol{p}_d = [0\ 0\ 0]^T$, $\boldsymbol{\eta}_d = [0° \quad 0° \quad 0°]^T$
- $\boldsymbol{V}_2$: $\boldsymbol{p}_d = [2\ 0\ 0]^T$, $\boldsymbol{\eta}_d = [-18° \quad 0° \quad 0°]^T$
- $\boldsymbol{V}_3$: $\boldsymbol{p}_d = [2\ 3\ 0]^T$, $\boldsymbol{\eta}_d = [-18° \quad 12° \quad 0°]^T$
- $\boldsymbol{V}_4$: $\boldsymbol{p}_d = [2\ 3\ 1]^T$, $\boldsymbol{\eta}_d = [-18° \quad 12° \quad 9°]^T$
- $\boldsymbol{V}_5$: $\boldsymbol{p}_d = [2\ 0\ 1]^T$, $\boldsymbol{\eta}_d = [-18° \quad 12° \quad 0°]^T$
- $\boldsymbol{V}_6$: $\boldsymbol{p}_d = [2\ 0\ 0]^T$, $\boldsymbol{\eta}_d = [-18° \quad 0° \quad 0°]^T$
- $\boldsymbol{V}_7$: $\boldsymbol{p}_d = [0\ 0\ 0]^T$, $\boldsymbol{\eta}_d = [0° \quad 0° \quad 0°]^T$

which were traveled along with rest-to-rest motions with maximum linear/angular velocities of 0.3 m/s and $15°/\text{s}$, and maximum linear/angular accelerations of 0.2 m/s^2 and $5°/\text{s}^2$. Figures 10(a–d) show the desired trajectory $(\boldsymbol{p}_d(t),\ \boldsymbol{\eta}_d(t))$, and the tracking errors $(\boldsymbol{e}_p(t),\ \boldsymbol{e}_R(t))$. The same initial condition as in Section VI-A is considered. The optimized value of $\alpha' = 26.5°$ and $\beta' = 19°$ for this trajectory obtained from Sec. IV has been used. Here it is clearly illustrated that at the vertex $\boldsymbol{V}_4$ the hexarotor exploits the 6 DoFs which is one of the main objectives of this titled propeller architecture. Note again how the tracking errors are kept to minimum (in power of 10^{-5}) despite the more complex motion involving several reorientations of the propellers. This confirms again the validity of the controller proposed in the previous Section III.

The interested reader can refer to the video attached to the paper for a more exhaustive illustration of the hovering and

[3]Here, for the sake of clarity, we represent orientations by means of the classical roll/pitch/yaw Euler set $\boldsymbol{\eta} \in \mathbb{R}^3$.

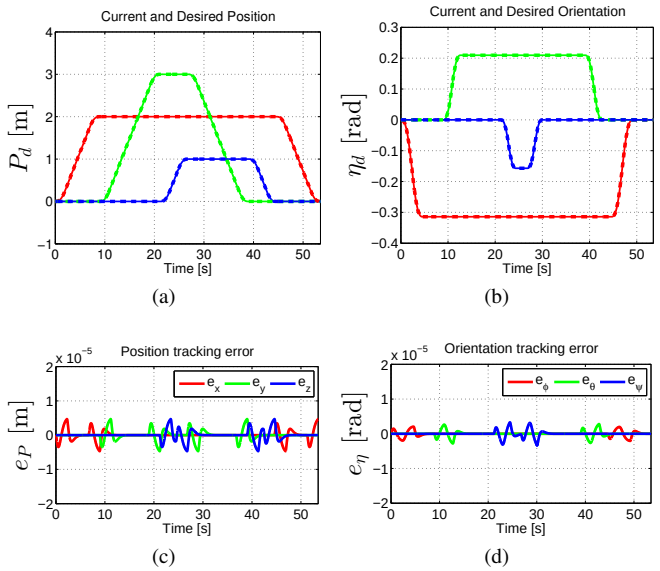

Fig. 10: Results of the robust 6 DoFs trajectory tracking. 10(a): Desired (dashed line) and current (solid line) position $\boldsymbol{p}_d$ in x(red), y(green) and z(blue). 10(b): Desired (dashed line) and current (solid line) orientation $\boldsymbol{\eta}_d$ in roll(red), pitch(green) and yaw(blue). 10(c–d): behavior of the position/orientation tracking errors $(\boldsymbol{e}_p, \boldsymbol{e}_\eta)$.

6 DOF hexarotor motion capabilities.

VII. CONCLUSIONS AND FUTURE WORKS

In this paper, we have overcome the underactuation, modeling and control issues for a standard UAV with a tilted propeller hexarotor architecture where the propellers can be rotated both w.r.t. X-axis and Y-axis. This concept allows to (i) gain full controllability over the 6 DoFs hexarotor pose in free space, and (ii) optimize the propeller tilt angle with respect to a minimum control effort over a desired trajectory. Carefully analyzing the controllability properties of the dynamic model, resulted in the hexarotor design being combined with trajectory tracking controller based on feedback linearization techniques. A clear validation of the controller's robustness is proved by means of extensive simulations.

Our future works are aimed at (i) developing robust control designs based on different non-linear techniques (e.g., sliding mode, backstepping) for robust stability analysis, (ii) realizing the prototype of the proposed tilted propeller hexarotor in order to experimentally validate the ideas discussed in this paper. Further research is mandatory for feasibility of $\boldsymbol{u}$. In addition, we are also, (iii) proceeding in the direction of optimizing the tilt angle to get a desired force $(\boldsymbol{F}_x, \boldsymbol{F}_y, \boldsymbol{F}_z \in \mathbb{R}^3)$ and desired torque $(\boldsymbol{T}_x, \boldsymbol{T}_y, \boldsymbol{T}_z \in \mathbb{R}^3)$ along the 3 principal body axes $\{\boldsymbol{X}_B,\ \boldsymbol{Y}_B,\ \boldsymbol{Z}_B\}$, which is the futuristic objective for any physical UAV interaction with the environment.

REFERENCES

[1] A. Franchi, C. Secchi, M. Ryll, H. H. Bülthoff, and P. Robuffo Giordano, "Shared control: Balancing autonomy and human assistance with a group of quadrotor UAVs," *IEEE Robotics & Automation Magazine, Special Issue on Aerial Robotics and the Quadrotor Platform*, vol. 19, no. 3, pp. 57–68, 2012.

[2] L. Marconi, R. Naldi, and L. Gentili, "Modeling and control of a flying robot interacting with the environment," *Automatica*, vol. 47, no. 12, pp. 2571–2583, 2011.

[3] G. Gioioso, M. Ryll, D. Prattichizzo, H. H. Bülthoff, and A. Franchi, "Turning a near-hovering controlled quadrotor into a 3D force effector," in *2014 IEEE Int. Conf. on Robotics and Automation*, Hong Kong, China, May. 2014, pp. 6278–6284.

[4] B. Yüksel, C. Secchi, H. H. Bülthoff, and A. Franchi, "Reshaping the physical properties of a quadrotor through IDA-PBC and its application to aerial physical interaction," in *2014 IEEE Int. Conf. on Robotics and Automation*, Hong Kong, China, May. 2014, pp. 6258–6265.

[5] ——, "A nonlinear force observer for quadrotors and application to physical interactive tasks," in *2014 IEEE/ASME Int. Conf. on Advanced Intelligent Mechatronics*, Besançon, France, Jul. 2014, pp. 433–440.

[6] P. E. I. Pounds, D. R. Bersak, and A. M. Dollar, "Grasping from the air: Hovering capture and load stability," in *2011 IEEE Int. Conf. on Robotics and Automation*, Shanghai, China, May 2011, pp. 2491–2498.

[7] Q. Lindsey, D. Mellinger, and V. Kumar, "Construction of cubic structures with quadrotor teams," in *2011 Robotics: Science and Systems*, Los Angeles, CA, Jun. 2011.

[8] G. Gioioso, A. Franchi, G. Salvietti, S. Scheggi, and D. Prattichizzo, "The Flying Hand: a formation of uavs for cooperative aerial telemanipulation," in *2014 IEEE Int. Conf. on Robotics and Automation*, Hong Kong, China, May. 2014, pp. 4335–4341.

[9] R. Naldi, L. Gentili, L. Marconi, and A. Sala, "Design and experimental validation of a nonlinear control law for a ducted-fan miniature aerial vehicle," *Control Engineering Practice*, vol. 18, no. 7, pp. 747–760, 2010.

[10] K. T. Oner, E. Cetinsoy, M. Unel, M. F. Aksit, I. Kandemir, and K. Gulez, "Dynamic model and control of a new quadrotor unmanned aerial vehicle with tilt-wing mechanism," *Int. Journ. of Mechanical, Aerospace, Industrial and Mechatronics Engineering*, vol. 2, no. 9, pp. 12–17, 2008.

[11] F. Kendoul, I. Fantoni, and R. Lozano, "Modeling and control of a small autonomous aircraft having two tilting rotors," *IEEE Trans. on Robotics*, vol. 22, no. 6, pp. 1297–1302, 2006.

[12] A. Sanchez, J. Escareño, O. Garcia, and R. Lozano, "Autonomous hovering of a noncyclic tiltrotor UAV: Modeling, control and implementation," in *17th IFAC World Congress*, Seoul, South Korea, Jul 2008, pp. 803–808.

[13] G. R. Flores, J. E. no, R. Lozano, and S. Salazar, "Quad-tilting rotor convertible MAV: Modeling and real-time hover flight control," *Journal of Intelligent & Robotics Systems*, vol. 65, no. 1-4, pp. 457–471, 2011.

[14] S. Salazar, H. Romero, R. Lozano, and P. Castillo, "Modeling and real-time stabilization of an aircraft having eight rotors," *Journal of Intelligent & Robotics Systems*, vol. 54, no. 1-3, pp. 455–470, 2008.

[15] M. Ryll, H. H. Bülthoff, and P. Robuffo Giordano, "Modeling and control of a quadrotor UAV with tilting propellers," in *2012 IEEE Int. Conf. on Robotics and Automation*, St. Paul, MN, May 2012, pp. 4606–4613.

[16] R. Voyles and G. Jiang, "Hexrotor UAV platform enabling dextrous interaction with structurespreliminary work," in *2012 IEEE Int. Symp. on Safety, Security and Rescue Robotics*, College Station, TX, Nov. 2012, pp. 1–7.

[17] V. Mistler, A. Benallegue, and N. K. M'Sirdi, "Exact linearization and noninteracting control of a 4 rotors helicopter via dynamic feedback," in *10th IEEE Int. Symp. on Robots and Human Interactive Communications*, Bordeaux, Paris, France, Sep. 2001, pp. 586–593.

[18] A. De Luca and G. Oriolo, "Trajectory planning and control for planar robots with passive last joint," *The International Journal of Robotics Research*, vol. 21, no. 5-6, pp. 575–590, 2002.

[19] M. Ryll, H. H. Bülthoff, and P. Robuffo Giordano, "First flight tests for a quadrotor UAV with tilting propellers," in *2013 IEEE Int. Conf. on Robotics and Automation*, Karlsruhe, Germany, May 2013, pp. 295–302.

[20] T. Lee, M. Leoky, and N. H. McClamroch, "Geometric tracking control of a quadrotor UAV on SE(3)," in *49th IEEE Conf. on Decision and Control*, Atlanta, GA, Dec. 2010, pp. 5420–5425.

[21] Y. Cheon, D. Lee, I.-B. Lee, and S. W. Sung, "A new PID autotuning strategy with operational optimization for MCFC systems," in *9th Asian Control Conference*, Istanbul, Turkey, Jun. 2013, pp. 1–6.